Design of a Two-Speed LAVT for Energetic Optimization of an Accessible Prosthetic Hand

Côme Butin, Damien Chablat, Yannick Aoustin, David Gouaillier

Côme Butin
Laboratoire des Sciences du Numérique de Nantes (LS2N), UMR CNRS 6004, & ORTHOPUS
Assistive technology manufacturer
Nantes, FRANCE
email: come.butin@orthopus.com

Damien Chablat[1]
LS2N, UMR CNRS 6004,
Nantes, FRANCE
email: damien.chablat@cnrs.fr

Yannick Aoustin
LS2N, UMR CNRS 6004,
University of Nantes, FRANCE
email: yannick.aoustin@univ-nantes.fr

David Gouaillier
ORTHOPUS,
Assistive technology manufacturer
Nantes, FRANCE
email: david.gouaillier@orthopus.com

Design of a Two-Speed Load Adaptive Variable Transmission for Energetic Optimization of an Accessible Prosthetic Hand

This work proposed the design of a simple, robust and inexpensive motion transmission for hand prostheses. The main challenge to be solved is to generate not only fast movements for the closing of the fingers during the grasping but also important forces to hold these objects. A Two-Speed Load Adaptive Variable Transmission is introduced to solve this challenge using a planetary gear train to reduce the speed and a selector clutch with wrap spring. The main properties of these two systems are recalled and a guideline is introduced to reach the user requirement. Finally, an application example is presented and the proposed prototype is analyzed.

Keywords: Hand prosthesis, motion transmission, wrap spring

1 Introduction

Myoelectric hand prostheses are developed since the 1970s to our days in various forms. The first myoelectric prostheses were designed with one Degree of Actuation (DoA) and were suitable to realize only the tridigital pinch. Tridigital hands such as the VariPlus Speed from Ottobock manufacture[2] or the Myo Kinisi hand from Steeper manufacture[3] are still sold, and are usually appreciated for their force, their speed and their robustness. The most advanced commercially available prostheses have more complex kinematics with up to six actuators and sub-actuation mechanisms to drive 10 or 11 joints, like the i-Limb Touch Bionics from Össur manufacture[4], the hand prosthesis from TASKA manufacture[5], and the hand prosthesis from COVVI manufacture[6]. These prostheses are more anthropomorphic, but are developing less force and speed [1] than the tridigital prostheses, and the system complexity leads to a lack of mechanical robustness. Their price is prohibiting for countries without a powerful health care system.

In the aim of designing an accessible prosthetic hand (affordable, easy-to-use, robust, easy-to-repair), limiting the number of actuators seems to be a legitimate choice by decreasing the complexity of the hand, thus reducing its price and the weight of the battery, increasing the robustness, and reducing the control strategy complexity for the user. Few commercial hands exist as hybrid between polydigital and tridigital hands with one or two actuators, such as the Michelangelo from Ottobock manufacture, the MyHand from Hy5 manufacture[7] and the Adam's Hand from BionIT Labs manufacture[8]. These prostheses remain complex, and cannot be afforded in low and middle income countries (LMIC).

A lot of academic works proposed single actuator prostheses [2–7]. These works are focusing on sub-actuation mechanisms and differential mechanisms to adapt the force exerted by each finger on the grasped object. Their pinching forces are poor (from 3.5N [3] to 34.5N [4] - only power grasp is documented in [7]) compared to the 78N measured on the Michelangelo [1] and the minimum 68N prescribed for Activities of Daily Living (ADL) [8]. Their speed is also poor (0.47s [3] to 1.4s [4] of closing time) compared to the performances of the commercially available hands (300mm/s, ~0.3s closing time for the Michelangelo and the VariPlus Speed). It can be noted that the fastest hand of the previous references is the weakest in terms of applicable efforts, while the one that applies the strongest efforts is the slowest.

Using more powerful motors to achieve better performance is not a reliable option. Increasing the motor power means increasing the cost of the prosthesis, its weight, its dimensions, and the size and weight of the battery system. Instead, the optimization of the energy consumption is preferred.

Considering that most of the energy is lost by Joule effect in the motor and mechanical friction, higher performances can be obtained with a same amount of energy by optimizing the transmission of the system and the operating point of the motor. Indeed, a myoelectric hand is working at two different operating points. For each grasp sequence, the open hand is firstly closing its fingers at a given speed with no external load until the object contacts the fingers. Then, the fingers apply an important force to securely hold the object, at very low speed. This characteristic is useful to optimize the energy consumption.

As pointed out in [8] many years ago, Ottobock strategy is to use an "automatic transmission", changing gear ratio when a high torque is detected by a spring. To the best author's knowledge, Ottobock equivalent solutions have never been analyzed in the academic literature, but patents have been submitted [9]. The developed system transforms a multi-turn rotary movement into a second multi-turn rotary movement. This mechanism needs an important number of complex and miniature mechanical parts, requiring precision machining.

Another solution can be inspired by the different types of Continuous Variable Transmission (CVT) where the reduction ratio is varying continuously with the transmitted torque. Most of the CVT have been developed for automotive industry, and their working principle is not suitable for affordable prosthesis where the num-

[1]Corresponding Author.
July 6, 2022
[2]https://www.ottobock.fr
[3]https://www.steepergroup.com
[4]https://www.ossur.com
[5]https://www.taskaprosthetics.com
[6]https://www.covvi.com
[7]https://www.hy5.no
[8]https://www.bionitlabs.com

ber and size of parts must be minimized to meet weight, size and price requirements. Only few different CVT have been proposed for prosthetic hands and robotics [10].

Takaki proposed a Rotary-to-Rotary CVT based on a five-bar linkage and a preconstrained spring [11]. While this system allows for a threefold increase in maximum finger force for a same input power and with pretty simple manufactured parts, this linkage does not provide a constant behavior on the finger range. A singularity appears for a particular position of the fingers, and the mechanism impacts directly all the hand kinematics. More recently, Liu adapted this linkage using a slider crank mechanism [12], with a force gain between two and four along the finger range. While the singularity has been removed, force magnification does not stay constant and is suitable only for prosthetic hands using translation movement.

Belter proposed a Rotary-to-Linear CVT [13] using a mechanism adapted from a lead screw where the pitch can vary depending on the force applied on the screw. In this mechanism, the screw and the nut are composed of smooth components to enable pitch variation, and the sliding is avoided by applying an initial force between the contacting bodies. The solution is suitable only for prosthetic hands using translation movement, and the maximum mechanical efficiency is comprised between 18% and 30% that limits the benefit of this transmission.

Finally, different works have been developed for tendon-based transmission. Matsuhita *et al.* [14] and O'brien *et al.* [15] are using drums with a varying diameter to adapt the tension and the speed of the wounded wire to the load. Shin *et al.* [16] use an actuator that twist a two-wire tendon to transform a rotary motion into a linear motion. The transmission ratio can be adjusted by twisting the two wires between each other (small reduction) or around a shaft (high reduction). A mechanism is proposed to switch between two modes depending on load. Theses works are specific to tendon-based prostheses which is not preferred in commercial prostheses [1] for the difficulties of transmitting high forces with robustness.

Others solutions are using two actuators [8, 17] but are not presented here while adding a second actuator will increase cost, weight, complexity, and probably energy consumption.

To solve the energy consumption issue caused by the use of a single actuator and by the need for high performances, we propose here a novel Load Adaptive Variable Transmission (LAVT). This LAVT exhibits similar performances to Ottobock's solutions with a multi-turn Rotary-to-Rotary transmission and two different speeds, capable of varying its reduction ratio under a given load. Thus, this mechanism could be associated with all kind of transmissions that use rotary actuator as input. Since this mechanism has been designed in the aim to be as simple as possible, it is composed of only few simple mechanical parts. It is composed of a planetary gear train (PGT) working in two different modes, and a selector clutch using wrap spring clutch, which switches the working mode of the PGT at a given torque. The design steps have been detailed to enable the adaptation of the mechanism to other applications. A first prototype has been developed as a proof of concept.

This work was conducted in collaboration with the BionicoHand project [18], which aims to develop an accessible Open Source prosthesis with rigid fingers (no DIP and PIP joint) with one single actuator. However, the solution proposed in this paper is suitable for any prosthetic hand or robotic gripper with one DoA requiring high power for low energy consumption.

This paper is outlined as follows. The different parameters of motorization that minimize energy consumption are analyzed in Section 2, and we show the advantages of the LAVT. Then, an architecture of LAVT, and a method of size it according to specifications are proposed Section 3. Section 4, an experimental protocol on a developed prototype is proposed, and the results are detailed and discussed. Finally, Section 5 offers conclusions and direction for future work.

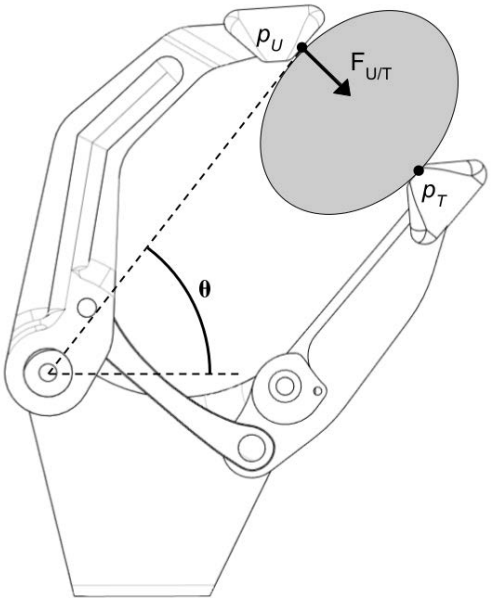

Fig. 1 Contact points p_U, p_T and force definition $F_{U/T}$ on a tridigital prosthetic hand

2 Design Constraints and Energy Analysis

2.1 Performances and User Needs. In a user-centric approach, it is important to start from the user needs. The prosthesis performances are a selection criterion for the user, but can also be a reason for prosthesis abandonment. In this work, we are interested in :

- the maximal opening width of the hand;
- the closing time, or the speed of the fingers;
- the grasping force and stability, which ensure to hold objects strongly.

It is important to keep in mind that the grasping stability is related to the grasping force, but also to other parameters such the material of the objects, the finger joints, the number of contact points or the distribution of the force between these points.

2.2 Grasping Force and Speed Definition. Grasping force and speed are key metrics to qualify the performances of robotic hands. While a metric to measure grasping stability is more complex to obtain, grasping force is also a key specification for the designer. These performances are often given by prosthesis manufacturers, but they are not clearly defined and seem to be different between companies and products.

A simple approach to define these metrics is to consider a pinch with two opposite groups of fingers (like a myoelectric gripper or a tridigital hand), with only two contact points located at finger tips. Thus, the analysis stays planar. Let us call p_U and p_T the contact points at tip of the upper fingers and the thumb respectively, and θ the position of the fingers, as shown on Fig. 1 for a tridigital prosthetic hand.

The linear speed V is defined as the approach speed between the two contact points p_U and p_T:

$$V(\theta) = \frac{\mathrm{d}\|\overrightarrow{p_U p_T}\|}{\mathrm{d}t} \tag{1}$$

Then, the pinching force is defined as the force exerted by the upper fingers on the thumb, equal and opposite to force exerted

by the thumb on the upper fingers. Considering the unit vector $\overrightarrow{u} = \frac{\overrightarrow{p_U p_T}}{\|p_U p_T\|}$,

$$F(\theta) = F_{U/T}\,\overrightarrow{u} \tag{2}$$

This choice is motivated by the aims of motorization sizing and optimization, since the grasping power $P_G(\theta)$ is equal to the product of the speed $V(\theta)$ and the force $F(\theta)$. This choice also allows to get rid of the kinematics and transmission between fingers in a first sizing iteration, since for a given constant torque and a constant rotation speed of the motorization, the grasping power P_G will no longer depend on θ, according to the principle of virtual power.

We can remark that these metrics are not suitable for hands with articulated fingers that enable more than two contact points on objects. In that case, a metric is proposed in [19], where our definition remains compatible in the case of two contact points.

2.3 Performance Index. An index is proposed in this section to characterize the needs for motorization sizing. The maximal grasping force F_{max} occurs when the object is grasped at very low speed, and the maximal speed V_{max} occurs in the approaching phase at very low load. On these two phases, the grasping power P_G previously introduced stands near to zero, it is not appropriate to size a motor and its reduction. We propose instead a Performance Index P_I, expressed in N.mm/s and defined as :

$$P_I = V_{max}(\theta) \cdot F_{max}(\theta) \quad \forall\theta \tag{3}$$

The performance index is valid for all angular values θ, but a single angular value θ has to be chosen to evaluate V_{max} and F_{max} at the same point, for example at mid-range, or for an object with a specific width.

According to the principle of virtual power, this performance index also characterizes the motor and its transmission in terms of maximal torque τ_{max} and maximal rotation speed ω_{max}, with $l_{eq}(\theta)$ the kinematic equivalent lever such that $V(\theta) = \omega \cdot l_{eq}(\theta)$, and thus $F(\theta) \cdot l_{eq}(\theta) = \tau$.

$$P_I = \frac{V_{max}(\theta)}{l_{eq}(\theta)} \cdot F_{max}(\theta) \cdot l_{eq}(\theta) = \omega_{max} \cdot \tau_{max} \tag{4}$$

In this way, the motor and its transmission can be sized independently of the kinematics.

2.4 Dissipated Energy at Grasp. A way to evaluate the minimal needed energy or power needed to grasp an object is to evaluate the power dissipated in an object due to its elasticity during grasping.

A grasping task does not require a high mechanical power, since speed is not necessary at the same time as force. It can be remarked that most of the grasped objects of daily life are highly rigid and are not storing or dissipating a lot of energy compared to the energy available in the battery. Considering an object as an elastic body, the work W to deform it can be from its stiffness coefficient K, its displacement variable Δx and F the force applied on it.

$$W = \frac{1}{2}K\Delta x^2 = \frac{F^2}{2K} \tag{5}$$

As an order of magnitude of the equation parameters, we selected a reusable polymer water cup to represent a low stiffness daily life object, and measured the work needed to grasp it with a force of 80N. By applying this force ten times on the border of the object, we measured an average displacement of 30mm, leading to a rough approximation of the stiffness coefficient K=2.5N/mm. This cup stores an energy W=1.3J, while a typical Li-ion Battery 7.2V 1000mAh is storing 26kJ, meaning 20'000 grasping tasks. Most of the objects are stiffer, and a force of 80N on a water cup to hold it firmly is voluntarily overestimated.

By squeezing this object in 0.3 seconds, a mean power of 4.3W will be necessary, while taking the maximal specifications of the Michelangelo (80N, 300mm/s) will lead to a power of 24W.

2.5 Power Analysis in Motor and Transmission. In the previous analyses, we showed that only few energy is needed for grasping, and that the Performance Index can ensure to attain the desired performances down to the reduction ratio, independently of the kinematics. We analyze in this section the effect of each parameter of the motorization in order to optimize the energy consumption while attaining desired performances.

The chosen model of motorization is composed of a brushed DC motor for its affordability and its simplicity of control, and a transmission composed of several stages of geared reducers.

The DC motor is characterized by its back-EMF constant k_E, approximately equal to its torque constant $k_M \approx k_E = K$, and its resistance R. The values of maximal torque and associated maximal current mainly come from the thermal limits of the motor, although the motor maximal thermal current can be exceeded over a short time with an adapted control strategy. The maximal admissible speed provides the maximal supply voltage. The transmission is characterized by its global reduction ratio $R_g = \omega_{out}/\omega_{mot}$ and its global efficiency coefficient η_g.

Assuming that the energy loss is negligible during the approach and that back EMF is negligible at grasping, we can compare the electrical power P_E consumed by the motor at stall condition with the Performance Index of the system.

$$P_E = RI_{max}^2 = R\frac{\tau_{mot,max}^2}{k_M^2} = \frac{R}{K^2}\frac{R_g^2}{\eta_g^2}\tau_{max}^2 \tag{6}$$

An Energy Loss Index E_{LI} can be introduced:

$$E_{LI} = \frac{P_E}{P_I} = \frac{R}{K^2}\frac{R_g^2}{\eta_g^2}\frac{\tau_{max}}{\omega_{max}} \tag{7}$$

To minimize E_{LI} according to Eq. (7), different terms can be minimized. The first term R/K^2 corresponds to the motor parameters. It has been observed that this term stays approximately constant (around 10 to 20% of variation) for different models, different nominal voltages and different coefficients K, on a given technology of brushed DC motor and for a given range of power. Taking care of minimizing this value during motor choice can be a good reflex, but it will not be a major factor.

The second term R_g^2/η_g^2 corresponds to transmission parameters. A first intuitive lever is the maximization of the mechanical efficiency η_g. It can be remarked that the effect is squared, so low efficiency transmissions like worm gear reducers have to be avoided. The reduction ratio R_g also plays an important role. An important reduction is needed to minimize E_{LI}, that is to say a motor with a low torque and a high speed. However, the speed is limited by the mechanical components used, and the motor used near its speed limit (around 9000 to 10000 RPM for classical DC brushed motors). It has to be kept in mind that a high speed lowers the lifetime of the motor, which can be a design issue.

Finally, the third term $\frac{\tau_{max}}{\omega_{max}}$ is fixed by the specifications and cannot be changed.

2.6 Introduction of Variable Transmission. The previous analysis shows that an optimization of some parameters is possible to reduce energy consumption at given performances. However, the minimization is limited at some point by the cost of improving efficiency and by the maximal speed of affordable motors.

Other solutions have been implemented, by varying the reduction ratio R_g between the approach phase ($R_g = R_I$) and the grasping phase ($R_g = R_{II}$). In these conditions, Eq. (7) is changed as

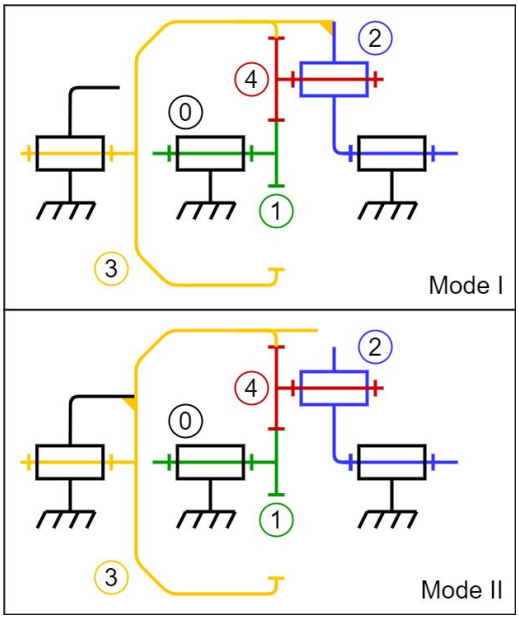

Fig. 2 LAVT kinematics diagram in mode I when ② and ③ are locked (no reduction) and mode II when ⓪ and ③ are locked (reduction)

follows:

$$E_{LI} = \frac{P_E}{P_I} = \frac{R}{K^2}\frac{R_{II}^2}{\eta_g^2}\frac{\tau_{max}}{\omega_{max}} \tag{8}$$

In this case, the minimization of R_{II} is no longer limited directly by the motor speed. With the ratio variation $Q = R_I/R_{II}$, R_I can be lowered by a factor of Q to maintain the same output speed without exceeding the motor maximal speed. The minimization of E_{LI} is then by a factor of Q^2. For example, a ratio variation of five between the two phases can lower the energy consumption by 25 while keeping same performances for the user. This result highly motivates the development of a variable transmission presented in the next sections.

3 Load Adaptative Variable Gear Train Analysis

3.1 Mechanism Principle and Architecture. The Load Adaptive Variable Transmission presented in this paper is a two-speed reducer where a transition between two speeds occurs when the transmitted torque is exceeding a predefined torque. The LAVT is based on a planetary gear train where parts can be blocked together or let free through a clutch, activated by the transmitted torque. Figure 2 shows the kinematic diagram in the two different modes. The planetary gear train is composed of the chassis ⓪, the sun gear ①, the carrier ②, the ring gear ③ and the satellites ④. The sun gear acts as the mechanism input. The carrier acts as the output.

In mode I, for low transmitted torque, the ring gear ③ is blocked on the carrier ②. It produces that the sun gear, the satellites, the carrier and the ring gear are fixed together. There is no reduction in mode I.

In mode II, for high transmitted torque, the ring gear ③ is blocked on the chassis ⓪. The speed ratio R of the planetary train in mode II is given by the following equation:

$$R = \frac{\omega_{out}}{\omega_{in}} = \frac{\tau_{in}}{\tau_{out}} = \frac{Z_1}{Z_3 + Z_1} \tag{9}$$

where τ_{in} and τ_{out} are the input and output torques, respectively and ω_{int} and ω_{out} are the input and output angular velocities, respectively of the planetary gear train, Z_1 is the number of teeth on the sun gear and Z_3 on the ring gear. The reduction ratio does not depend on the number of the teeth Z_4 of the satellites .

The torque ratio of the PGT is $1/R$ when considering negligible the friction losses on the teeth.

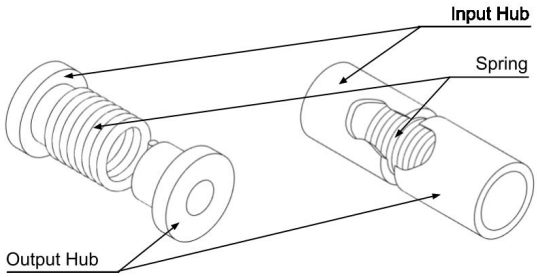

Fig. 3 Overrunning clutch using wrap spring clutch, external (left) or internal (right)

3.2 Selector Clutch using Wrap Spring Clutch. This LAVT relies on a selector clutch that locks the ring gear either on ring gear or carrier depending on the transmitted torque. The developed clutch is based on wrap spring clutches.

Wrap spring clutches can be used in many applications, such as overrunning clutches (or one-way clutch), indexing clutches, or clutch brakes. It consists of a coil spring between two rotating bodies (input and output), where the bodies are in contact of the spring either on internal or external surfaces, as shown on Fig. 3 [20, 21]. Their working principle is standing on the Capstan effect [22] that permits to amplify a friction pressure along a coil by applying a small tension at one end. The resulting torque is increasing exponentially to the number of active coils N and the friction coefficient μ.

The simplest application of wrap spring clutches are overrunning clutches (Fig. 3) where the input can transmit high torque to the output in one way, and is slipping in the other way. In the free way, a small amount of friction has to be countered, while in the blocking way this friction is largely amplified. The initial frictional torque τ_0 can be produced by a counter torque at the free end. The slipping torque limit in the blocking way τ^b, which also depends on the spring wire radius r_s and the spring neutral radius r_n, is given by Cronin [22] in the following equation:

$$\tau^b = \tau_0 e^{2\pi N\mu\frac{\rho}{1+\rho}} \approx \tau_0 e^{2\pi N\mu} \quad \text{with} \quad \rho = \frac{r_n}{r_s} \gg 1 \tag{10}$$

The initial frictional torque can be either produced by a small interference δr between the spring internal radius $r_0 = r_n - r_s$ and the body radius r. The torque slipping limits have been expressed by Wiebusch [23] and Wahl [24] in blocking way τ^b and in the free way τ^f , considering an internal clutch with a high radius ratio ρ as follows.

$$\tau^b = \frac{EI}{r_n^2}\delta r(e^{2\pi N\mu} - 1) \tag{11}$$

$$\tau^f = \frac{EI}{r_n^2}\delta r(1 - e^{-2\pi N\mu}) \approx \frac{EI}{r_n^2}\delta r, \quad \text{with} \quad N\mu > 1 \tag{12}$$

where E and I represent, respectively, Young's modulus and the moment cross-section of the spring.

It has been noticed that in the blocking way, measurements can lead to errors with respect to the results given by Eq. (11) up to 20% [23]. Several problems can explain differences such as chosen

hypotheses [24] or friction coefficient variability [22]. In the free way, the theory is more reliable.

The curved beam theory [24] also gives us the radial displacement r_i for a free spring under a given torque τ_i in:

$$\tau_i = \frac{EI}{r_n^2}\delta r_i. \tag{13}$$

The form of this equation is similar to that of Eq. (12).

By using the same principle, it is possible to create a selector clutch by combining an internal clutch and an external wrap spring clutch on the same spring to switch between Mode I and Mode II. Figure 4 shows the profile of the spring. Under no load, the spring is preloaded on the body **A**. This preload creates a friction as shown in Eq. (12), which permits transferring low torque from surface **S** to **A**. When load is applied to the spring through body **S**, the spring is expanding in diameter until contacting the surface **B**. At this point, the friction on the surface **B**, greater than the slipping limit on the surface **A**, makes the spring block on the surface **B** while **A** begins to slip. This type of clutch selector is used in Ottobock's Greifer, combined with a more complex transmission than the simple PGT proposed here.

This selector clutch is working only in one way, where the spring is expanding under torque. In the other way, the spring will be blocked on the friction surface **A** that makes LAVT blocked in mode I. Thus, this working is acceptable for a grasping task, where high torque is only useful at the end of the fingers closing while opening can be realized at low torque only.

Wrap spring clutch seems to be an interesting technical solution for accessible prosthetic hand, with a good durability, a high torque to dimensions ratio and a low manufacturing cost [25].

3.3 Loads and Efficiency Analysis. Figure 5 introduces the different parts of the planetary gear train and the selector clutch combined together.

The torque applied by the satellites ④ on the ring gear ③, noted $\tau_{4/3}$ and the torque applied by the satellites ④ on the carrier ②, noted $\tau_{4/2}$ can be expressed from the torque applied by the satellites ④ on the sun shaft ①, noted $\tau_{4/1}$ at static equilibrium.

$$\tau_{4/3} = -\left(\frac{1}{R} - 1\right)\tau_{1/4} \tag{14}$$

$$\tau_{4/2} = \frac{1}{R}\tau_{1/4} \tag{15}$$

In mode I, when the spring is only in contact with the carrier, the output torque τ_{out} can be expressed from the input torque τ_{in} as follows:

$$\begin{aligned}\tau_{out} &= \tau_{3/2} + \tau_{4/2} = \tau_{4/3} + \tau_{4/2} \\ &= -\tau_{in}\left(\frac{1}{R} - 1\right) + \tau_{in}\frac{1}{R} = \tau_{in}\end{aligned} \tag{16}$$

In mode II, when the spring is contacting the chassis and is slipping on the carrier, the output torque can be expressed from the input torque as follows:

$$\tau_{out} = \tau^b_{3/2} + \tau_{4/2} = -\tau^b_{2/3} + \tau_{in}\frac{1}{R} \tag{17}$$

While input torque is entirely transmitted to the output in mode I, providing an efficiency coefficient $\eta = 1$ by assuming an ideal PGT, a constant friction torque remains in mode II. In this mode, the efficiency coefficient is expressed as follows:

$$\eta = \frac{P_{out}}{P_{in}} = \frac{\omega_{out}}{\omega_{in}}\frac{\tau_{out}}{\tau_{in}}$$

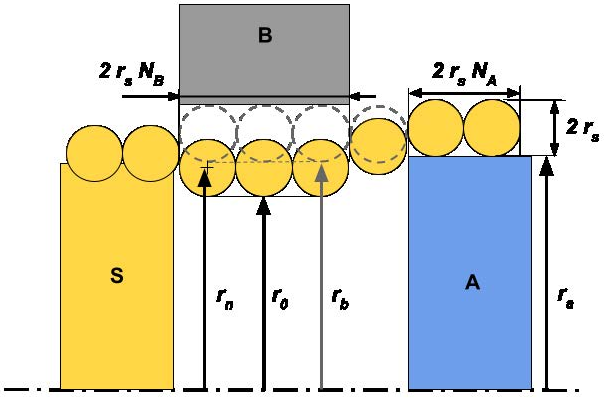

Fig. 4 Spring contact profile of Selector Clutch

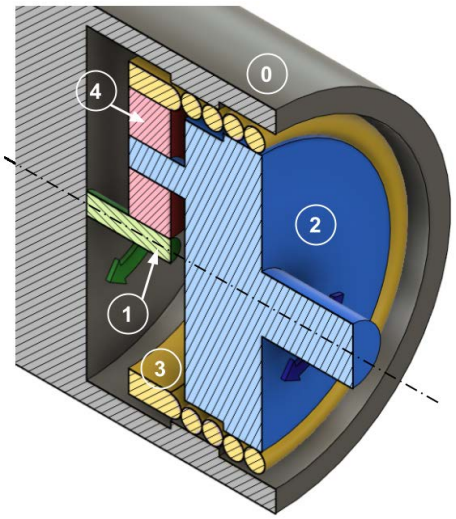

Fig. 5 Principle of the LAVT with the chassis ⓪, the input shaft or sun shaft ①, the carrier or output shaft ②, ring gear and the spring ③ and the satellites ④

$$= R\frac{\tau_{in}/R - \tau^b_{2/3}}{\tau_{in}} = \frac{\tau_{in} - \tau^b_{2/3}R}{\tau_{in}} \tag{18}$$

From Eq. (13), the torque on the spring needed to contact the surface **B** is known. This transition torque τ_t applied on the spring can be expressed as a transition torque from the input shaft:

$$\tau_{2/3} = \tau_t \Leftrightarrow \tau_{in} = \tau^t_{in} = \left(\frac{R}{1-R}\right)\tau_t \tag{19}$$

Figure 6 presents the output torque τ_{out} for a normalized input torque τ_{in} between zero and one, according to Eq. (16) and Eq. (17). Five different pairs of speed ratio R and τ_t are chosen to show the impacts of these two parameters. The sliding torque $\tau^b = \tau^b_{2/3}$ is set such that $\tau^b = \tau_t$ that is a result of the sizing process and corresponds to its optimal value as it will be explained in Section 3.4. Figure 6 shows that a higher output torque τ^{max}_{out} can be provided by decreasing R, or by decreasing the transition torque τ_t.

The efficiency is presented on Fig. 7 where $\eta = 1$ during the Mode I phase and η is calculated from Eq. (18) during the Mode II. The different configurations are plotted for a same range of the input torque τ_{in}, explaining the different ranges of τ_{out}. Figure 7 shows that the principal effect of decreasing R is an enlargement of the graph in mode II, corresponding to the higher increase rate

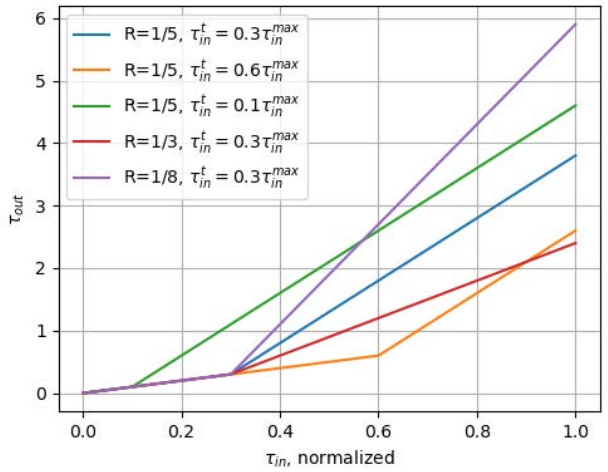

Fig. 6 τ_{out} as function of τ_{in} at quasi-static state for five different pairs of (R, τ_t), with $\tau^b = \tau_t$

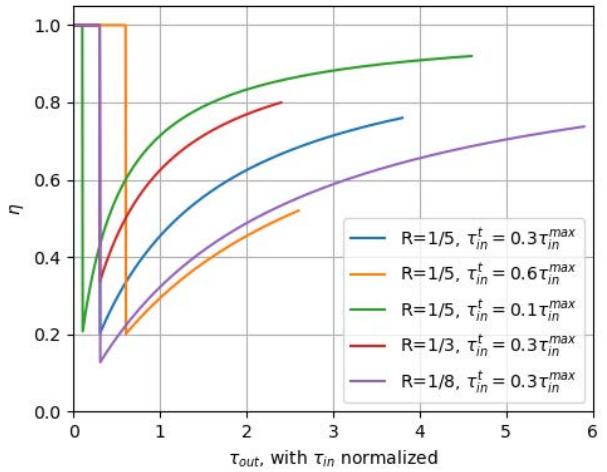

Fig. 7 η as function of τ_{out} at quasi-static state for five different pairs of (R, τ_t), with $\tau^b = \tau_t$

on Fig. 6. A slight decrease of the efficiency at output maximal torque can be noticed but stays small. Conversely, τ_{max}^{out} is highly degraded by an increase of the transition torque τ_t.

A first approach to optimize the energetic efficiency of this mechanism would be to minimize the reduction ratio and the transition torque.

3.4 Sizing Process. The sizing process is organized in five main steps.

Reduction ratio and transition of the torque. To size the system, the reduction ratio R and the transition torque τ_t have to be chosen. These two parameters are affecting the maximal torque available and the speed in mode II, but also the efficiency of the system, and the minimal torque available in mode I before transition (Eqs. (16)-(19)).

As seen in Section 3.3, it is advised to lower R and τ_t to obtain a high maximal output torque with a high efficiency. Thus, these two parameters have a lower limit.

A very low R is difficult to realize with a standard PGT (around 1/8). Furthermore, a too low value of R can lower the speed in mode II too much, producing a sensation of control loss by the user.

The transition torque at output τ_{out}^t should stay high enough to overcome friction and glove elasticity without speed loss.

Planetary gear train sizing. From the chosen reduction ratio, the planetary gear train can be sized. The number of teeth of the sun gear Z_1, of the satellites Z_4 and of the ring gear $Z_3 = 2Z_4 + Z_1$ are constrained:

- manufacturing process of gears and cost constrain the gears to have at least eight to ten teeth, and a module as high as possible;
- the radius of the ring gear should stay as low as possible to keep the volume of the mechanism low;
- the number of satellites N_{sat} is preferably three, or four. Using two satellites is less favorable for force distribution on sun gear, requiring bigger teeth and producing more vibrations. Using more than four satellites is not advised for limiting friction and keeping an efficient gearbox;
- assembly is possible only if $(Z_1 + Z_4) \mod N_{sat} = 0$;
- the radius, module and width of the gears should be adapted to the transmitted torque.

Under these constrains, all numerical values of the reduction ratio R given by Eq. (9) are not realizable, especially for $R < 1/5$.

Spring wire sizing. The wire diameter should be selected to handle the stress induced in the spring during deformation. When the spring is not contacting the outer ring, it can be represented as a curved beam subjected to a torque. The following equation gives the stress σ_{max} of a spring with an inertia I under a torque τ_{max}.

$$\sigma_{max} = \frac{r_s}{I} k_b \tau_{max} < R_e s \tag{20}$$

where s is a safety coefficient and R_e the elastic limit.

For circular section, it gives:

$$\sigma_{max} = \frac{4k_b}{\pi r_s^3} \tau_{max}. \tag{21}$$

Here k_b is the correction factor of the curved beam theory defined as:

$$k_b = \frac{4\rho^2 - \rho - 1}{4\rho(\rho - 1)} \quad \text{with} \quad \rho = \frac{r_n}{r_s} \tag{22}$$

While Eq. (22) involves r_n which has not been determined yet, an approximation of k_b can be used in a first iteration. For $\rho > 8$, taking $k_b = 1.1$ permits to respect Eq. (20).

The wire diameter should be kept as low as possible to maximize a displacement under a given torque, and thus reducing the needed manufacturing precision. A further analysis is needed to validate the stress in the spring under constraints on the outer ring.

Spring diameter and friction surfaces sizing. Once the wire diameter is selected, the spring diameter and the diameter of the two friction surfaces can be chosen.

The transition torque τ_t can be expressed from Eq. (13) and the radius r_b of the contact surface **B**.

$$\tau_t = \frac{EI}{r_n^2} \delta r_b \tag{23}$$

The input and output torques at transition τ_{in}^t and τ_{out}^t can be expressed:

$$\tau_{in}^t = \tau_{out}^t = \frac{REI}{(1-R) r_n^2} \delta r_b \tag{24}$$

Thus, for a given torque, different parameter pairs $(r_n, \delta r_b)$ can be chosen. Choosing a high δr_b can improve the robustness of the

system with respect to manufacturing inaccuracies, but increases the volume of the system.

To ensure contact, the spring has to contact body **B** before sliding on body **A**. At sliding condition, the intermediate portion of spring will attain an internal radius equal to r_b. Radius r_a has to be set as close as possible of r_b to reduce the friction torque τ^b down to τ_t, but it has to stay greater with a small clearance to ensure a correct transition. This torque is calculated with Eq. (12) and is slightly higher than the transition torque τ_t.

$$\tau^b = \frac{EI}{r_n^2}\delta r_a \tag{25}$$

Spring length and material choice. When the spring is contacting the body **B**, sliding torque between **S** and **A** has to be lower than sliding torque between **S** and **B**, as follows:

$$\frac{EI}{r_n^2}\delta r_a < \frac{EI}{r_n^2}\delta r_b(\mathrm{e}^{2\pi N_B \mu} - 1) \tag{26}$$

with N_A and N_B representing the number of spires contacting surfaces **A** and **B** respectively.

The interference radius δr_a and δr_b are set close to each other, so a simplification can be made.

$$\mathrm{e}^{2\pi N_B \mu} > 2 \Leftrightarrow N_B \mu > \frac{\ln(2)}{2\pi} \approx 0.11 \tag{27}$$

In mode II, the torque between the spring and the surface **B** should stay under the sliding limit expressed in Eq. (10) with $\tau_0 = \tau^b$ the friction torque between the spring and the surface **A**.

$$\tau^b(\mathrm{e}^{2\pi N_B \mu} - 1) > \tau_{in}^{max}\frac{1-R}{R} \tag{28}$$

In the opening direction, the torque applied on the spring should stay under the sliding limit expressed in Eq. (11).

$$\tau^b(\mathrm{e}^{2\pi N_A \mu} - 1) > \tau_{in}^{max}\frac{1-R}{R} \tag{29}$$

These three conditions on μ, N_A, and N_B have to be respected. While the choice of material acts on μ, it stays constrained to common materials (steel, aluminum, bronze to keep the mechanism affordable).

3.5 Numerical Application. In this work a myoelectric hand with high performances (80N, 300mm/s) is considered. Considering kinematics from a tridigital hand as shown on Fig. 1 with an equivalent lever l_{eq}=130mm and assembled with a geared reduction between LAVT and fingers of 1/26, several objectives and constraints have been set:

- a maximal input torque τ_{in}^{max} = 100N.mm given by the motor and the first stages of reduction;
- a minimal transition torque τ_{out}^{t} > 15N.mm to overcome the frictions and glove elasticity;
- a maximal output torque τ_{out}^{max} = 400N.mm needed for the power grasp of 80N;
- a speed reduction at mode switch $\omega_I/\omega_{II} \geq 5$ to keep sufficient speed while grasping;
- an efficiency at maximal torque $\eta(\tau_{out}^{max}) > 80\%$, induced by the last objectives and compatible with the energy optimization goal.

Parameters	Config. 1	Config. 2	Config. 3	Chosen
τ_{in}^{max}	—	100N.mm	—	✓
R	—	1/5	—	✓
τ_{in}^{t}	17N.mm	17N.mm	19.5Nmm	✓
τ_t	68N.mm	68N.mm	78N.mm	
τ_{out}^{max}	432N.mm	418N.mm	418N.mm	
$\eta(\tau_{out}^{max})$	86.4%	83.6%	83.6%	
ω_I/ω_{II}	—	5	—	
N_{sat}	—	3	—	✓
Z_4	—	48	—	✓
Z_3	—	12	—	
Z_1	—	18	—	
r_s	—	0.5mm	—	
δr_b	0.5mm	0.5mm	0.575mm	✓
r_n	—	8.7mm	—	
δr_a	0.5mm	0.6mm	0.6mm	✓
N_A	—	2	—	
N_B	—	3	—	

Table 1 Sizing results of configuration studied

Three different configurations have been chosen with different dimensions of friction surfaces, in order to test the influence of these dimensions. The results are presented in Table 1, where the column "Chosen" specifies the parameters chosen by the designer to meet the specifications, and the other parameters arising from the chosen ones. The material used for spring and frictions surface is steel.

Similarly to Figs. 6 and 7, the input to output characteristic and the efficiency coefficient of the three configurations are shown in Fig. 8. R is constant in the three configurations, while τ_t and τ^b are varying with δr_a and δr_b. We observe a plateau between mode I and mode II for two of these configurations on Fig. 8 (left), created by a sliding torque τ^b bigger than the transition torque τ_t, induced by $\delta r_a > \delta r_b$. On this plateau, the spring does not slip on surface **A** nor on surface **B**, which blocks the mechanism. The efficiency is not defined in this interval, Fig. 8 (right). Using a DC motor as input with a simple voltage control, this interval does not seem to cause any problems. Indeed, while the mechanism will tend to block, the motor output torque will increase rapidly as a response of speed decrease, and pass the interval.

The efficiency is supposed to be maximal (η=1) in Mode I, while there is no sliding of the spring and the others possible frictions are neglected, as shown in Eq. (16).

4 Experimentations

4.1 LAVT Prototype Overview. A first functional prototype has been designed as a proof of concept to validate the theoretical model developed in the last section. The functional parts (spring, friction surfaces, gears) of the prototype are designed at scale for further integration in a prosthesis, but the overall prototype has been designed to be manufactured and assembled easily. The friction ring including surface **B** and the friction hub including surface **A** attached to the carrier are changeable to permit experiments with different diameter friction surfaces. The chassis is partially transparent to allow seeing all parts moving. A section view of a CAD and a picture of the prototype are presented in Figs. 9 and 10.

4.2 Experimental Setup. Measurements have been conducted to validate the input-output characteristic of Fig. 6 in quasi-static working state, at low speed. From this characteristic, the transition torque τ_t and the friction torque in mode II $\tau_{2/3}^b$ can be

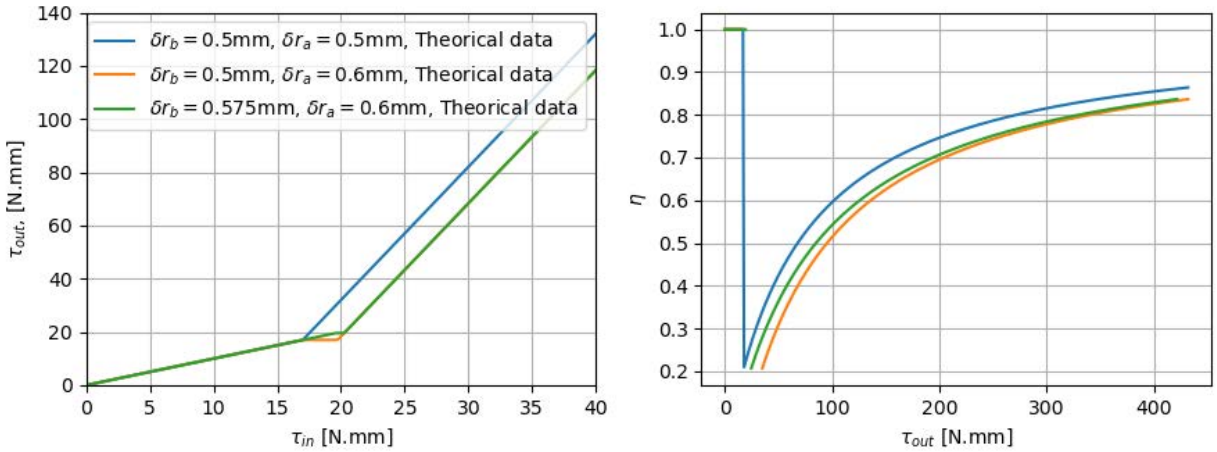

Fig. 8 τ_{in} **as function of** τ_{out} **(left) and** η **as function of** τ_{out} **(right) of the three selected configurations**

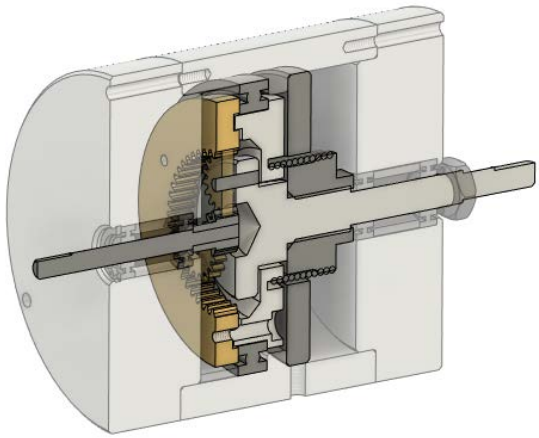

Fig. 9 Section view of LAVT (CAD)

identified.

As shown on Fig. 11, a constant load torque is applied to the output shaft through a pulley and a predetermined mass M. The input shaft and its pulley are driven by the experimenter at a constant low speed through a cable and a force sensor, giving the torque applied on the input shaft. The force sensor is a Micro Load Cell (Phidgets CZL616C), and the corresponding signal is amplified and acquired using a PhidgetBridge module. For each output torque given by an output mass M, the measured input torque is acquired and averaged along several turns to get a mean value of the input torque. A range of masses from 2.0g to 385.0g and two 3D printed pulleys ⌀50mm are used to apply output torques from 0N.mm to 95N.mm. This setup should be consolidated before testing greater torques. However the range chosen is sufficient to show the transition between the two working modes of the LAVT.

Measuring the viscous friction and the efficiency at given speed would be interesting, but requires adapted measurement tools that we do not have access to.

4.3 Results. Figure 12 shows the signal acquired by the force sensor. The load cell has been calibrated before the measurements to compensate the weight of the pulley and taking into account the cable angle. It can be seen on Fig. 12 that the noise in not negligible. However, taking the average value limits the impact of the noise on the measure.

We also observe that a non-constant residual friction torque appears and varies on an entire turn (visible on the Fig. 12 for $M = 31.5$g). It has been noticed that when the spring begins to expand under load before the transition, the spring can touch slightly the outer ring on one side if all parts are not perfectly centered. It creates a residual friction torque.

Figure 13 shows the results of the experiment compared to the theoretical data. A first order interpolation of experimental data is also plotted.

Slip and stick. A slip and stick effect appears in mode II between the spring and the carrier. This effect can be avoided by playing with materials, surface roughness or lubrication.

Screw effect. When the spring is slipping of the carrier in mode II, its helicoidal shape creates a force with tends to stretch itself. While a counter-force from the spring rigidity can limit the spring extension, it can be not sufficient to keep the spring at its right place in the assembly.

"Dead turn". Even if the dynamic behavior of the LAVT is out of the scope of this first analysis, it is interesting to observe that the spring needs to be preloaded before transition when a torque is applied on the output shaft. Thus, when the output shaft is blocked by an object, the input shaft has to turn several turns before actually shift the LAVT to mode II. The number of spring turns before transition ΔN_t can be calculated through the stiffness of the spring and the number N_f of free spires:

$$\Delta N_t = \frac{N_f r_n}{EI} \tau_t \tag{30}$$

When the carrier is stopped, the movement of the spring and ring gear will be amplified by the PGT, such as the number of turns ΔN_t^{in} of the input shaft will be larger.

$$\Delta N_t^{in} = \frac{1-R}{R} \Delta N_t = \frac{1-R}{R} \frac{N_f r_n}{EI} \tau_t \tag{31}$$

For $N_f = 6$ in our prototype, we have $\Delta N_t^{in} = 1.36$tr. This "dead turn" can create a delay for the user which has to be taking into account, but also limits the shocks on the motor shaft when the fingers contact an object.

Configurations comparison and discussion. From Tab 2, the configuration 2 seems to be most interesting to use, with the highest maximal output torque τ_{out}^{max}. The configuration 1 shows the worst performances. These results do not correspond to the expected results of Tab. 1 and Fig. 8, where configuration 1 has the best performances and configuration 2 has the worst.

Tolerances, manufacturing process, surfaces roughness, lubrication and assembly conditions are varying with each configuration,

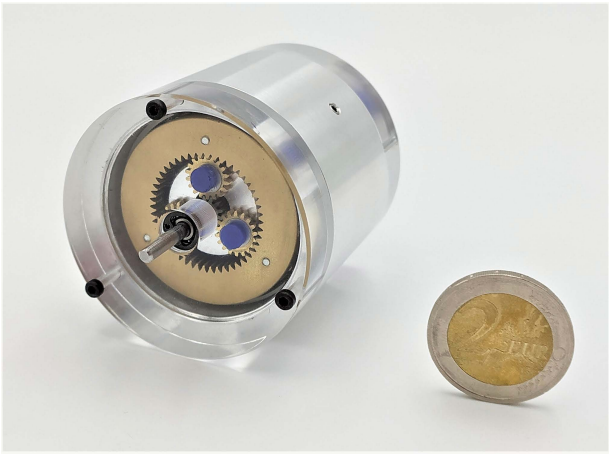

Fig. 10 Picture of LAVT Prototype

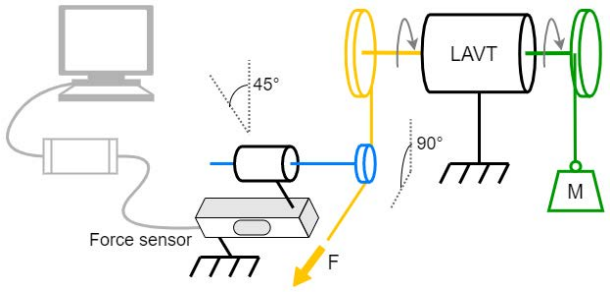

Fig. 11 Experimental setup diagram for analysis of the quasi-static input to output characteristic

and could explain the differences between theoretical and experimental results. The effects of such changes will have to be investigated in the further studies by repeating measurements in different conditions. In particular, a second prototype with separated PGT and selector clutch could help to identify the friction sources and to test the different configurations of the selector clutch without a complete disassembly of the PGT. The manufacturing precision of the gears and the spring have also to be improved for better performances.

With a better knowledge of the manufacturing tolerances needed in this application, the manufacturing costs could be optimized for a commercialized prosthetic hand.

Additional frictions. From the interpolation, we can easily observe additional frictions. Table 2 shows the friction torques calculated from interpolations. These frictions can easily be explained:

- in mode I, dry frictions can appear from the bearings on the input shaft, the output shaft and the ring gear;
- in mode II, dry frictions can appear from bearings but also from the gears of the PGT which is activated.

5 Conclusions and Future Works

This paper reports an analysis of the energy consumption for hand prostheses and a step-by-step method to size the transmission mechanism for a given specification for the prostheses. The aim of this project is to provide innovative solutions for accessible prosthetic hand with high performances and low energy consumption.

A prototype has been manufactured and assembled, and the operating principle of the mechanism has been validated theoretically and experimentally. The numerical tests and the experimentation show that the transition torque can be controlled as desired, and

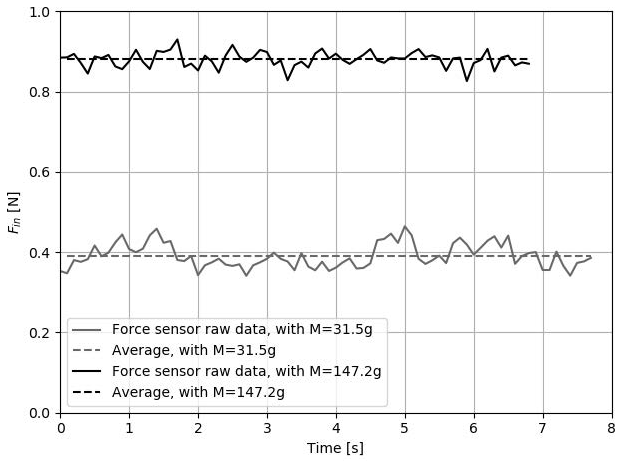

Fig. 12 Force sensor raw data for two different output masses for Configuration 1

that this force amplification system seems to be useful, even with unwanted additional friction.

This mechanism could help designing accessible and powerful prosthetic hands. With a constant energy consumption, using this mechanism can multiply the grasping force by four without changing the speed, or double both speed and grasping force with a constant energy consumption. This feature can offer to the user a more useful prosthesis for daily life activities. This mechanism could be used more generally in all embedded systems that require both speed and force at different times, and where energy efficiency, weight and cost are constrained, such as mobile robots performing grasping tasks.

About perspective this prototype produced could be improved to reduce the residual friction. Indeed, differences between theoretical and experimental results were observed. The effects of parameters not taken into account in the model such as assembly conditions or lubrication are suspected, but further study is needed.

The future work of this project will also consist in writing a dynamic model of the mechanism to take into account the effect of the springs. Secondly, a study of the robustness and fatigue resistance can be carried out. Finally, the integration of this mechanism into a global non-backdrivable transmission will be necessary.

Funding Data

This research was supported by ANRT CIFRE grant n°2019/1721, which funded the first author's doctoral studies.

Conflict of Interest

There are no conflicts of interest.

References

[1] Belter, J. T., Segil, J. L., Dollar, A. M., and Weir, R. F., 2013, "Mechanical design and performance specifications of anthropomorphic prosthetic hands: A review," The Journal of Rehabilitation Research and Development, **50**(5), pp. 599–618.

[2] Belter, J. T. and Dollar, A. M., 2013, "Novel differential mechanism enabling two DOF from a single actuator: Application to a prosthetic hand," *2013 IEEE 13th International Conference on Rehabilitation Robotics (ICORR)*, IEEE, Seattle, WA USA, pp. 1–6, doi: 10.1109/ICORR.2013.6650441.

[3] Leddy, M. T. and Dollar, A. M., 2018, "Preliminary Design and Evaluation of a Single-Actuator Anthropomorphic Prosthetic Hand with Multiple Distinct Grasp Types," *2018 7th IEEE International Conference on Biomedical Robotics and Biomechatronics (Biorob)*, IEEE, Enschede, pp. 1062–1069, doi: 10.1109/BIOROB.2018.8487198.

[4] Wattanasiri, P., Tangpornprasert, P., and Virulsri, C., 2018, "Design of Multi-Grip Patterns Prosthetic Hand with Single Actuator," IEEE Transactions on Neural Systems and Rehabilitation Engineering, **26**(6), pp. 1188–1198.

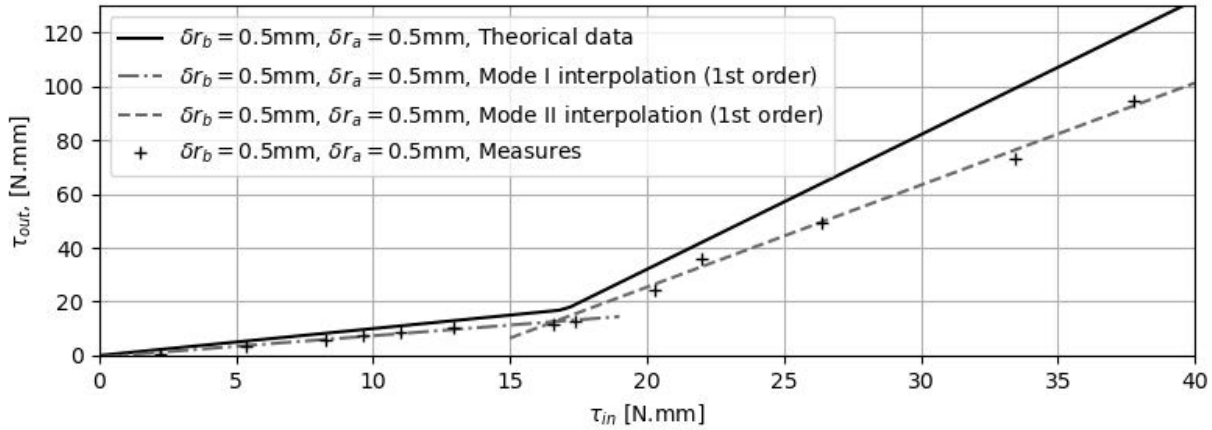

Fig. 13 Comparison of theoretical and experimental input-output torque characteristic of Configuration 1

Parameter	Config. 1	Config. 2	Config. 3
$(\delta r_a, \delta r_b)$	(0.5, 0.5)mm	(0.6, 0.5)mm	(0.6, 0.575)mm
Mode I identification (1st order)	$\tau_{out} = 0.79\tau_{in} - 0.56$	$\tau_{out} = 0.87\tau_{in} - 1.84$	$\tau_{out} = 0.80\tau_{in} - 0.38$
Mode I constant friction torque	0.56N.mm	1.84N.mm	0.38N.mm
Mode I proportional losses	21%	13%	20%
Mode II identification (1st order)	$\tau_{out} = 3.79\tau_{in} - 50.4$	$\tau_{out} = 4.09\tau_{in} - 65.0$	$\tau_{out} = 4.07\tau_{in} - 64.5$
Mode II constant friction torque	50.4N.mm	65.0N.mm	64.5N.mm
Mode II proportional losses	24%	18%	18%
Estimation of τ_{out}^{max}	329N.mm	344N.mm	343N.mm

Table 2 Identification of residual friction losses

[5] Zheng, Y., Li, X., Tian, L., and Li, G., 2018, "Design of a Low-Cost and Humanoid Myoelectric Prosthetic Hand Driven by a Single Actuator to Realize Basic Hand Functions," *2018 IEEE International Conference on Cyborg and Bionic Systems (CBS)*, IEEE, Shenzhen, pp. 603–606, doi: 10.1109/CBS.2018.8612255.

[6] Xu, K., Liu, H., Zenghui Liu, Du, Y., and Zhu, X., 2015, "A single-actuator prosthetic hand using a continuum differential mechanism," *2015 IEEE International Conference on Robotics and Automation (ICRA)*, IEEE, Seattle, WA, USA, pp. 6457–6462, doi: 10.1109/ICRA.2015.7140106.

[7] Laffranchi, M., Boccardo, N., Traverso, S., Lombardi, L., Canepa, M., Lince, A., Semprini, M., Saglia, J. A., Naceri, A., Sacchetti, R., Gruppioni, E., and De Michieli, L., 2020, "The Hannes hand prosthesis replicates the key biological properties of the human hand," Science Robotics, **5**(46), p. eabb0467.

[8] Weir, R. F., 2004, "Design of Artificial Arms and Hands for Prosthetic Applications," *Standard Handbook of Biomedical Engineering & Design*, Digital engineering library mcgraw-hill ed., pp. 32.1 – 32.61.

[9] Puchhammer, G., 2007, "Clutch module for prostheses," WO2007076795A1.

[10] Kernbaum, A. S., Kitchell, M., and Crittenden, M., 2017, "An ultra-compact infinitely variable transmission for robotics," *2017 IEEE International Conference on Robotics and Automation (ICRA)*, IEEE, Singapore, Singapore, pp. 1800–1807, doi: 10.1109/ICRA.2017.7989212.

[11] Takaki, T., Sugiyama, K., Takayama, T., and Omata, T., 2006, "Development of a 2-d.o.f. finger using load-sensitive continuously variable transmissions and ultrasonic motors," Advanced Robotics, **20**(8), pp. 897–911.

[12] Liu, H., Bin, Z., Liu, Z., and Xu, K., 2020, "Design of a Lightweight Single-Actuator Multi-Grasp Prosthetic Hand with Force Magnification," Journal of Mechanisms and Robotics, **12**(5), pp. 1–33.

[13] Belter, J. T. and Dollar, A. M., 2014, "A Passively Adaptive Rotary-to-Linear Continuously Variable Transmission," IEEE Transactions on Robotics, **30**(5), pp. 1148–1160.

[14] Matsushita, K., Shikanai, S., and Yokoi, H., 2009, "Development of Drum CVT for a wire-driven robot hand," *2009 IEEE/RSJ International Conference on Intelligent Robots and Systems*, IEEE, St. Louis, MO, USA, pp. 2251–2256, doi: 10.1109/IROS.2009.5354239.

[15] O'Brien, K. W., Xu, P. A., Levine, D. J., Aubin, C. A., Yang, H.-J., Xiao, M. F., Wiesner, L. W., and Shepherd, R. F., 2018, "Elastomeric passive transmission for autonomous force-velocity adaptation applied to 3D-printed prosthetics," Science Robotics, **3**(23), p. eaau5543.

[16] Shin, Y. J., Lee, H. J., Kim, K.-S., and Kim, S., 2012, "A Robot Finger Design Using a Dual-Mode Twisting Mechanism to Achieve High-Speed Motion and Large Grasping Force," IEEE Transactions on Robotics, **28**(6), pp. 1398–1405.

[17] Naclerio, N. D., Kerst, C. F., Haggerty, D. A., Suresh, S. A., Singh, S., Ogawa, K., Miyazaki, S., Cutkosky, M. R., and Hawkes, E. W., 2019, "Low-Cost, Continuously Variable, Strain Wave Transmission Using Gecko-Inspired Adhesives," IEEE Robotics and Automation Letters, **4**(2), pp. 894–901.

[18] "Projets: Bionicohand WIKILAB (accessed in November 2021)," https://wikilab.myhumankit.org/index.php?title=Projets:Bionicohand

[19] Falco, J., Van Wyk, K., and Messina, E., 2018, "Performance Metrics and Test Methods for Robotic Hands," doi: 10.6028/NIST.SP.1227-draft.

[20] Lowery, R. and Mehrbrodt, A., 1976, "How to do more with wrapped-spring clutches," Machine Design, **48**(17), pp. 78–83, Publisher: Penton Publ Inc 1100 Superior Ave, Cleveland, OH 44114.

[21] Roach, G. M. and Howell, L. L., 2002, "Evaluation and comparison of alternative compliant overrunning clutch designs," J. Mech. Des., **124**(3), pp. 485–491.

[22] Cronin, K. and Gleeson, J. P., 2013, "Variability in output torque of capstan and wrap spring elements," Mechanism and Machine Theory, **68**, pp. 49–66.

[23] Wiebusch, C. F., 1939, "The Spring Clutch," Journal of Applied Mechanics, **6**(3), pp. A103–A108.

[24] Wahl, A. M., 1940, "Discussion: "The Spring Clutch" (Wiebusch, C. F., 1939, ASME J. Appl. Mech., 6, pp. A103–A108)," Journal of Applied Mechanics, **7**(2), pp. A89–A91.

[25] King, R. and Monahan, R., 1999, "Alternator Pulley with Integral Overrunning Clutch for Reduction of Belt Noise," *SAE Technical Paper*, pp. 1999–01–0643, doi: 10.4271/1999-01-0643.

,